



LWS/TIM
NASA Ames
May 2014

The New RADMHD: A CGEM Global 3D Radiative-MHD Model of the Convection Zone-to-Corona System

W.P. Abbett, D.J. Bercik

The Basic Challenge:

It is evident that active region magnetic fields (and solar magnetic fields in general) span the entirety of the convection-zone-to-corona system, and do not exist in isolation in a localized region, or interact only over a prescribed spatial scale. The challenge of modeling the system in its entirety is that the magnetic field spans regions whose physical conditions vary dramatically:

(1) The convection zone is a high- β , optically-thick, high density plasma with energy transport dominated by convective motions, while the solar corona is a low- β , optically-thin, sparse, hot, magnetically-dominated plasma.

(2) The two regimes are physically connected through an interface region spanning the photosphere, chromosphere, and transition region. In these layers, the plasma transitions from optically-thick to optically-thin, from high to low- β in a highly-stratified environment that spans (on average) 4 orders of magnitude in temperature, and 12 to 13 orders of magnitude in density.

Numerical codes tend to be designed to treat different regions of the combined system separately, yet recent observations and numerical models show that the corona and surface layers are deeply interconnected through the atmospheric ***“interface region.”***

Physical regimes

Corona: hot, low- β , optically thin, shocks, field-aligned electron thermal conduction, non-thermal physics, short timescales

Transition region: optically thin, magnetically-dominated, steep temperature gradients, shocks, restrictive energy scale height (conduction)

Chromosphere: optically thin to continuum radiation, optically thick to energetically important atomic transitions, non-LTE radiative transport, a mixture of low and high- β plasma, convectively stable, shocks

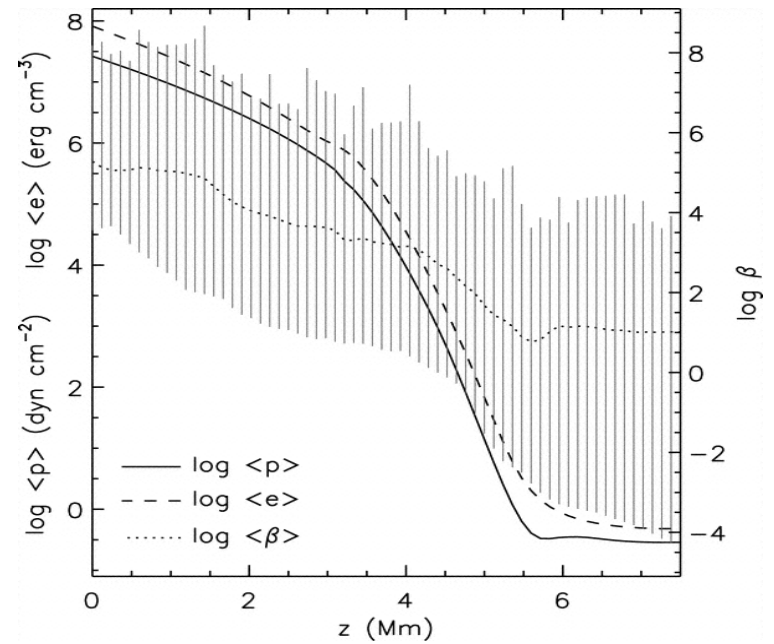
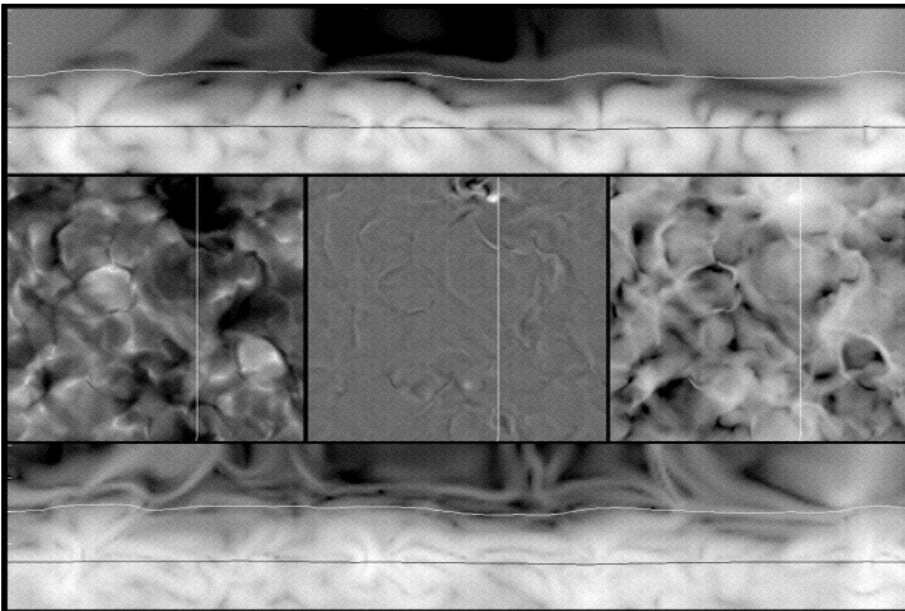
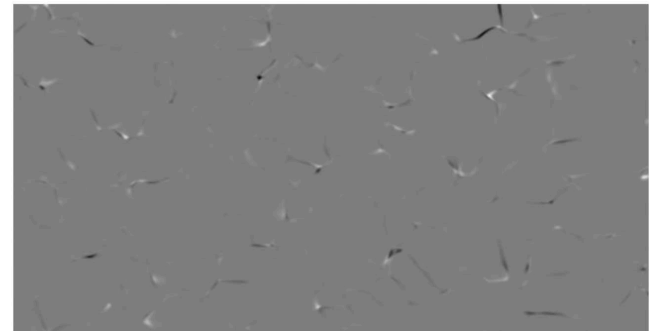
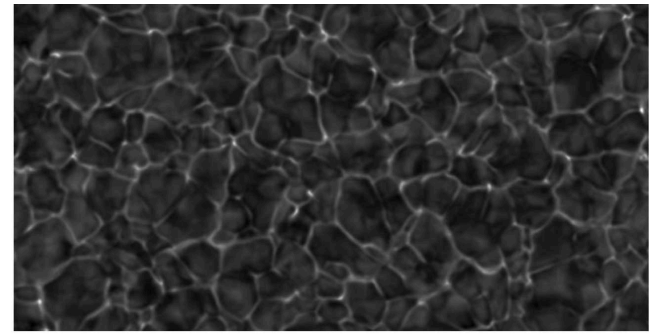
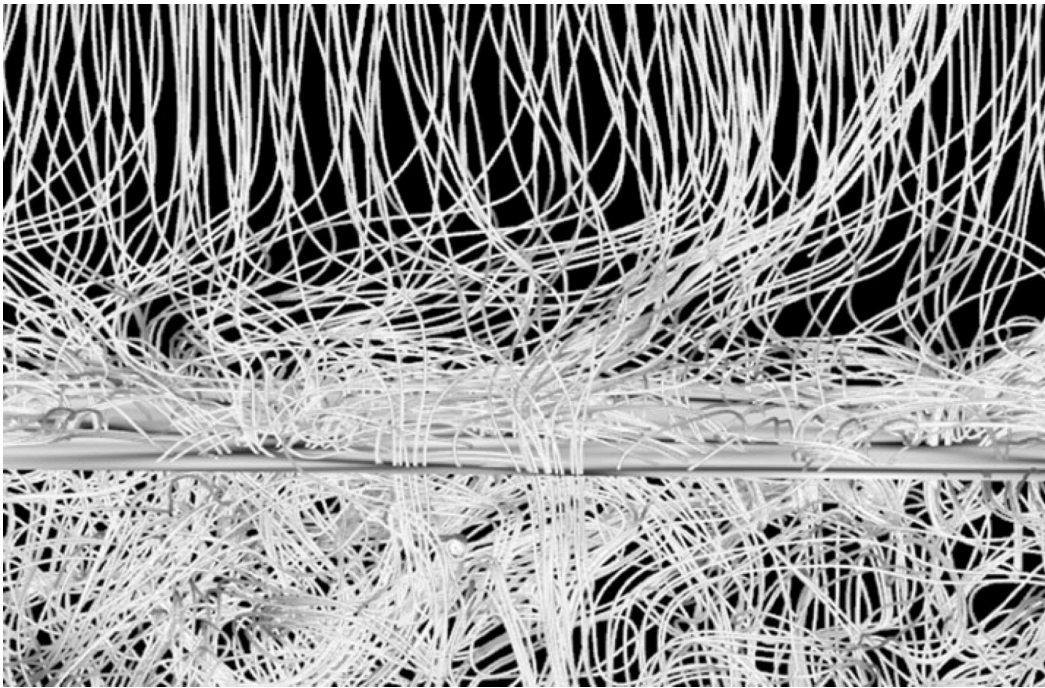
Surface layers: $\beta \approx 1$ (strong fields), transition from convective to radiative energy transport, overshoot layer, highly stratified, pressure scale height ~ 100 km

Upper convection zone: $\beta \geq 1$, optically thick, convectively unstable, compressible MHD required

Deep convection zone: high- β , convectively unstable, optically-thick, long timescales, $v/c_s \ll 1$, $v_a < c_s$

Visible surface





The Basic Challenge:

As magnetic fields emerge into the solar atmosphere, their observed properties span a wide range of spatial and temporal scales. For example, active region fields observed in the corona are rarely in isolation --- they are often connected to other ARs some distance away on the solar disk, and always emerge into a global magnetic field whose structural complexity is a function of the solar cycle.

Yet even small-scale events (such as the emergence of flux at granular or supergranular scales) can trigger rapid changes in the large-scale coronal field that are sufficient to trigger eruptive events. Time scales of the coupled system range from seconds during flares, to months as AR magnetic flux emerges, evolves, and decays.

As a modeling community, we have made great progress in better describing the energy sources and sinks in the CZ-to-corona system; for example, the physics of radiation transport at small scales in the complex interface region, or the effects of local cross-field diffusion in chromospheric plasmas. *Yet very little effort has been directed at addressing the fundamental problem of cross-scale coupling, and improving solar models by updating their underlying discretization formalism.*

CGEM Dynamic Models: RADMHD

To expand the scope of convection zone-to-corona models, and address the challenge of dynamically and energetically coupling large-scale active region and global magnetic fields with the small scale structure associated with realistic turbulent convection at and below the visible surface, we have updated and improved the underlying numerical formalism of RADMHD.

$$\frac{\partial \rho}{\partial t} + \nabla \cdot (\rho \mathbf{u}) = 0$$

$$\frac{\partial \rho \mathbf{u}}{\partial t} + \nabla \cdot \left[\rho \mathbf{u} \mathbf{u} + \left(p + \frac{B^2}{8\pi} \right) \mathbf{I} - \frac{\mathbf{B} \mathbf{B}}{4\pi} - \mathbf{D} \right] = \rho \mathbf{g}$$

$$\frac{\partial \mathbf{B}}{\partial t} + \nabla \cdot (\mathbf{u} \mathbf{B} - \mathbf{B} \mathbf{u}) = -\nabla \times \eta (\nabla \times \mathbf{B})$$

$$\frac{\partial e}{\partial t} + \nabla \cdot (e \mathbf{u}) = -p \nabla \cdot \mathbf{u} + \frac{\eta}{4\pi} |\nabla \times \mathbf{B}|^2 + \varphi + Q$$

Closure relation: a non-ideal equation of state obtained through an inversion of a tabular equation of state

Much of the important physics of the system is contained in the energy source term, Q

The new implementation of RADMHD is an efficiently-parallelized, semi-implicit radiative-MHD solver that advances the conservative portion of the MHD system of equations by means of a high-order, non-directionally-split 3D semi-discrete explicit scheme, while incorporating certain energy sources into the system via an implicit Jacobian-Free Newton Krylov solver.

RADMHD energetics:

RADMHD treats resistive dissipation, viscous stresses, and most other energy sources in the implicit sub-step, using an efficient “Jacobian-free” Newton-Krylov solver. Energy sources in the RADMHD model corona include field-aligned electron thermal conduction, and radiative losses in the optically-thin limit.

The code now calculates optically-thick radiative cooling by approximating the solution to the gray (frequency-independent) radiative transfer equation in local thermodynamic equilibrium (LTE) assuming a local, plane-parallel geometry. *This approximation of optically-thick surface cooling provides significant, and necessary computational savings for large-scale simulations, but is less realistic than those models that solve the frequency-dependent transfer equation in detail.*

However, our goal is to evolve the system with sufficient realism over the spatial scales necessary to investigate the interaction of small-scale surface convection with large-scale magnetic structures present in the global corona, and *couple dynamics at different scales within the highly-stratified thermodynamic transition between the convective interior and atmosphere*

We now focus on improvements to RADMHD’s underlying discretization scheme that allow us to pursue this objective.

Global RADMHD: Developments and improvements

Spherical geometry and a block non-uniform mesh. RADMHD can now evolve the system of MHD conservation equations on a spherical polar coordinate, *block non-uniform* mesh, either globally or over an AR-scale spherical wedge.

Fully-3D interpolation and direct stabilization. RADMHD code is no longer directionally split; its semi-discrete, finite-volume formalism now calculates fluxes using a high-order, 3D, 27-point piecewise continuous interpolating polynomial. *This allows flows and shocks to be propagated more accurately in off-axis directions.* The CWENO scheme has been replaced by a new, *much more robust* method of shock stabilization that uses a normalized, direct measure of flux discontinuities along control volume faces.

High-order treatment of vector fields. Many directionally-split finite volume schemes treat vector components like scalar fields. *In curvilinear coordinate systems, this treats mutable unit vectors as constants resulting in 1st-order accuracy.* Therefore, unless the cell volumes are small in extent (i.e., Cartesian-like), accuracy is poor. To overcome this challenge, we decompose vector fields into their Cartesian components so that unit vectors can be integrated, but still perform the integrations in spherical geometry.

Global RADMHD: Developments and improvements

Tensor fluxes for vector fields. A high-order Gaussian integration is now used when integrating fluxes over a control volume to update cell averages. The order of accuracy of the discretization scheme is maintained by using a tensor formalism to integrate the vector conservation equations (momentum, and magnetic fields) over a curvilinear mesh element. The advantage of a tensor flux scheme is that there are no geometric source terms that arise from integrating a vector field component-by-component. *Such source terms can introduce errors because they are not calculated in the same way numerical fluxes are calculated.*

Constrained transport. To eliminate any divergence error in the magnetic field, we extended the method of Kissmann & Pomoell (2012) to 3D curvilinear geometries and incorporated it into RADMHD. This constrained transport scheme is formulated to ensure that electric fields at face edges are consistent between cell volumes that share an edge. Given an initially divergence-free magnetic field, this scheme maintains the solenoidal constraint to within numerical round-off error while also conserving magnetic flux and accurately propagating discontinuities in the magnetic field.

Scaling: The MHD state vector can now be easily be scaled to accommodate local or global problems. The scaled variables are defined as a variable in cgs units divided by either a dimensioned scaling factor or dimensionless reference value. This simple feature is important for global calculations.

Vector momentum conservation -- finite volume tensor formulation:

$$\frac{1}{\Delta V} \int_V \frac{\partial \mathbf{p}}{\partial t} dV + \frac{1}{\Delta V} \int_V \nabla \cdot \mathbf{T} dV = \frac{1}{\Delta V} \int_V \mathbf{S} dV$$

$$\frac{1}{\Delta V} \int_V \frac{\partial \mathbf{p}}{\partial t} dV = -\frac{1}{\Delta V} \oint_A \hat{\mathbf{n}} \cdot \mathbf{T} dA + \frac{1}{\Delta V} \int_V \mathbf{S} dV$$

where

$$\mathbf{T} = \frac{1}{\rho} \mathbf{p} \otimes \mathbf{p} - \frac{1}{4\pi} \mathbf{B} \otimes \mathbf{B} + \left(P + \frac{1}{8\pi} \mathbf{B} \cdot \mathbf{B} \right) \mathbf{I}$$

$$\Delta V = \int_V dV$$

$$\begin{aligned} \mathbf{p} &= p_r(r, \theta, \phi) \hat{\mathbf{r}} + p_\theta(r, \theta, \phi) \hat{\boldsymbol{\theta}} + p_\phi(r, \theta, \phi) \hat{\boldsymbol{\phi}} \\ &= p_x(r, \theta, \phi) \hat{\mathbf{x}} + p_y(r, \theta, \phi) \hat{\mathbf{y}} + p_z(r, \theta, \phi) \hat{\mathbf{z}} \end{aligned}$$

$$\begin{aligned} \mathbf{B} &= B_r(r, \theta, \phi) \hat{\mathbf{r}} + B_\theta(r, \theta, \phi) \hat{\boldsymbol{\theta}} + B_\phi(r, \theta, \phi) \hat{\boldsymbol{\phi}} \\ &= B_x(r, \theta, \phi) \hat{\mathbf{x}} + B_y(r, \theta, \phi) \hat{\mathbf{y}} + B_z(r, \theta, \phi) \hat{\mathbf{z}} \end{aligned}$$

Vector momentum conservation -- finite volume tensor formulation:

$$\frac{1}{\Delta V} \int_V \frac{\partial \mathbf{p}}{\partial t} dV = -\frac{1}{\Delta V} \oint_A \hat{\mathbf{n}} \cdot \mathbf{T} dA + \frac{1}{\Delta V} \int_V \mathbf{S} dV$$

where

$$\begin{aligned} \frac{1}{\Delta V} \oint_A \hat{\mathbf{n}} \cdot \mathbf{T} dA &= \frac{1}{\Delta V} \int_{A_r^L} (-\hat{\mathbf{r}}) \cdot \mathbf{T} dA_r + \frac{1}{\Delta V} \int_{A_r^U} \hat{\mathbf{r}} \cdot \mathbf{T} dA_r \\ &+ \frac{1}{\Delta V} \int_{A_\theta^L} (-\hat{\boldsymbol{\theta}}) \cdot \mathbf{T} dA_\theta + \frac{1}{\Delta V} \int_{A_\theta^U} \hat{\boldsymbol{\theta}} \cdot \mathbf{T} dA_\theta \\ &+ \frac{1}{\Delta V} \int_{A_\phi^L} (-\hat{\boldsymbol{\phi}}) \cdot \mathbf{T} dA_\phi + \frac{1}{\Delta V} \int_{A_\phi^U} \hat{\boldsymbol{\phi}} \cdot \mathbf{T} dA_\phi \end{aligned}$$

For example, at the lower r -face of a control volume,

$$\frac{1}{\Delta V} \int_{A_r^L} (-\hat{\mathbf{r}}) \cdot \mathbf{T} dA_r = -\frac{1}{\Delta V} \int_{A_r^L} \left[\frac{p_r}{\rho} \mathbf{p} - \frac{B_r}{4\pi} \mathbf{B} + \left(P + \frac{1}{8\pi} \mathbf{B} \cdot \mathbf{B} \right) \hat{\mathbf{r}} \right] dA_r$$

Since the outward normal vectors over faces of the control volume are not constant, we evaluate the integrals in the following way:

$$\begin{aligned}
\frac{\partial}{\partial t} \overline{p_x}(r, \theta, \phi) &= \frac{1}{\Delta V} \int_{A_r^L} [\sin(\theta) \cos(\phi) T_{rr}(r, \theta, \phi) + \cos(\theta) \cos(\phi) T_{r\theta}(r, \theta, \phi) - \sin(\phi) T_{r\phi}(r, \theta, \phi)] dA_r - \\
&\quad \frac{1}{\Delta V} \int_{A_r^U} [\sin(\theta) \cos(\phi) T_{rr}(r, \theta, \phi) + \cos(\theta) \cos(\phi) T_{r\theta}(r, \theta, \phi) - \sin(\phi) T_{r\phi}(r, \theta, \phi)] dA_r + \\
&\quad \frac{1}{\Delta V} \int_{A_\theta^L} [\sin(\theta) \cos(\phi) T_{\theta r}(r, \theta, \phi) + \cos(\theta) \cos(\phi) T_{\theta\theta}(r, \theta, \phi) - \sin(\phi) T_{\theta\phi}(r, \theta, \phi)] dA_\theta - \\
&\quad \frac{1}{\Delta V} \int_{A_\theta^U} [\sin(\theta) \cos(\phi) T_{\theta r}(r, \theta, \phi) + \cos(\theta) \cos(\phi) T_{\theta\theta}(r, \theta, \phi) - \sin(\phi) T_{\theta\phi}(r, \theta, \phi)] dA_\theta + \\
&\quad \frac{1}{\Delta V} \int_{A_\phi^L} [\sin(\theta) \cos(\phi) T_{\phi r}(r, \theta, \phi) + \cos(\theta) \sin(\phi) T_{\phi\theta}(r, \theta, \phi) - \sin(\phi) T_{\phi\phi}(r, \theta, \phi)] dA_\phi - \\
&\quad \frac{1}{\Delta V} \int_{A_\phi^U} [\sin(\theta) \cos(\phi) T_{\phi r}(r, \theta, \phi) + \cos(\theta) \sin(\phi) T_{\phi\theta}(r, \theta, \phi) - \sin(\phi) T_{\phi\phi}(r, \theta, \phi)] dA_\phi + \frac{1}{\Delta V} \int_V S_x(r, \theta, \phi) dV
\end{aligned}$$

$$\begin{aligned}
\frac{\partial}{\partial t} \overline{p_y}(r, \theta, \phi) &= \frac{1}{\Delta V} \int_{A_r^L} [\sin(\theta) \sin(\phi) T_{rr}(r, \theta, \phi) + \cos(\theta) \sin(\phi) T_{r\theta}(r, \theta, \phi) + \cos(\phi) T_{r\phi}(r, \theta, \phi)] dA_r - \\
&\quad \frac{1}{\Delta V} \int_{A_r^U} [\sin(\theta) \sin(\phi) T_{rr}(r, \theta, \phi) + \cos(\theta) \sin(\phi) T_{r\theta}(r, \theta, \phi) + \cos(\phi) T_{r\phi}(r, \theta, \phi)] dA_r + \\
&\quad \frac{1}{\Delta V} \int_{A_\theta^L} [\sin(\theta) \sin(\phi) T_{\theta r}(r, \theta, \phi) + \cos(\theta) \sin(\phi) T_{\theta\theta}(r, \theta, \phi) + \cos(\phi) T_{\theta\phi}(r, \theta, \phi)] dA_\theta - \\
&\quad \frac{1}{\Delta V} \int_{A_\theta^U} [\sin(\theta) \sin(\phi) T_{\theta r}(r, \theta, \phi) + \cos(\theta) \sin(\phi) T_{\theta\theta}(r, \theta, \phi) + \cos(\phi) T_{\theta\phi}(r, \theta, \phi)] dA_\theta + \\
&\quad \frac{1}{\Delta V} \int_{A_\phi^L} [\sin(\theta) \sin(\phi) T_{\phi r}(r, \theta, \phi) + \cos(\theta) \sin(\phi) T_{\phi\theta}(r, \theta, \phi) + \cos(\phi) T_{\phi\phi}(r, \theta, \phi)] dA_\phi - \\
&\quad \frac{1}{\Delta V} \int_{A_\phi^U} [\sin(\theta) \sin(\phi) T_{\phi r}(r, \theta, \phi) + \cos(\theta) \sin(\phi) T_{\phi\theta}(r, \theta, \phi) + \cos(\phi) T_{\phi\phi}(r, \theta, \phi)] dA_\phi + \frac{1}{\Delta V} \int_V S_y(r, \theta, \phi) dV
\end{aligned}$$

And finally,

$$\begin{aligned}
 \frac{\partial}{\partial t} \overline{p_z}(r, \theta, \phi) = & \frac{1}{\Delta V} \int_{A_r^L} [\cos(\theta) T_{rr}(r, \theta, \phi) - \sin(\theta) T_{r\theta}(r, \theta, \phi)] dA_r - \\
 & \frac{1}{\Delta V} \int_{A_r^U} [\cos(\theta) T_{rr}(r, \theta, \phi) - \sin(\theta) T_{r\theta}(r, \theta, \phi)] dA_r + \frac{1}{\Delta V} \int_{A_\theta^L} [\cos(\theta) T_{\theta r}(r, \theta, \phi) - \sin(\theta) T_{\theta\theta}(r, \theta, \phi)] dA_\theta - \\
 & \frac{1}{\Delta V} \int_{A_\theta^U} [\cos(\theta) T_{\theta r}(r, \theta, \phi) - \sin(\theta) T_{\theta\theta}(r, \theta, \phi)] dA_\theta + \frac{1}{\Delta V} \int_{A_\phi^L} [\cos(\theta) T_{\phi r}(r, \theta, \phi) - \sin(\theta) T_{\phi\theta}(r, \theta, \phi)] dA_\phi - \\
 & \frac{1}{\Delta V} \int_{A_\phi^U} [\cos(\theta) T_{\phi r}(r, \theta, \phi) - \sin(\theta) T_{\phi\theta}(r, \theta, \phi)] dA_\phi + \frac{1}{\Delta V} \int_V S_z(r, \theta, \phi) dV
 \end{aligned}$$

The updated components of the state vector (volume average quantities) are then projected back onto the spherical polar coordinate axes.

Advantage:

Using a tensor formalism to integrate the *vector* conservation equations over a curvilinear mesh element ***preserves the order of accuracy of the discretization scheme***. Angular momentum is conserved, and there are no geometric source terms that arise from integrating a vector field component by component.

Discretization and the 3D Semi-Discrete formalism

Determining the values of e.g., the momentum flux at the faces of a control volume would be a simple affair if we did not wish to account for mathematical discontinuities.

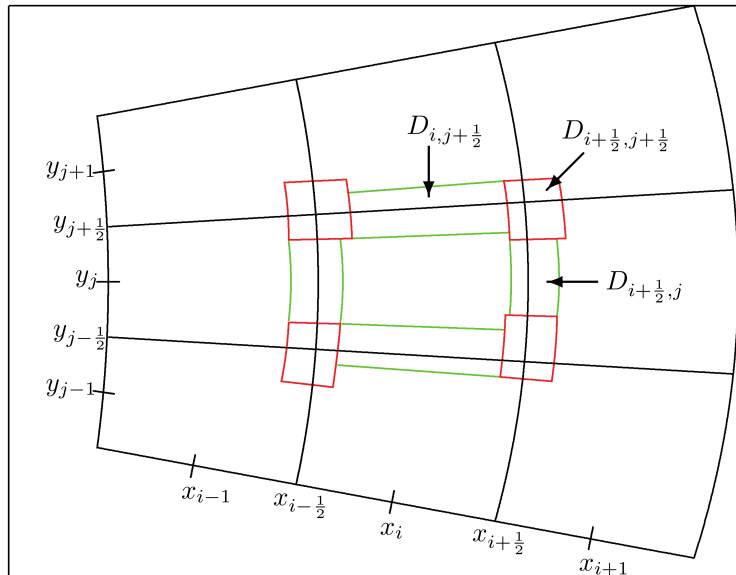


Figure from rom Illenseer & Duschl (2009)

However, discontinuities are physically important in a shock-dominated model atmosphere, and *capturing and evolving discontinuities frees us from having to cluster points in regions of steep evolving gradients* --- something commonplace in the CZ-to-corona system. We therefore construct a generalized solution to the 3D compressible MHD system in curvilinear coordinates.

Discontinuities must be evolved in a manner consistent with the evolution of continuous regions. Regions where discontinuities may occur (i.e., the faces edges and corners of control volumes where physical fluxes are calculated) intersect multiple control volume cells and can therefore be considered to be on a 'staggered' grid relative to the primary control volume.

To construct a generalized, discretized solution, we must reconstruct solutions in these staggered regions, evolve them, and then project them back onto the principal control volumes.

Discretization and the Semi-Discrete formalism

The mathematical formalism of our discretization scheme is described in detail in Abbett & Bercik (2014). Our approach essentially extends the method of Illenseer & Duschl (2009) to a fully 3D, non-directionally split, curvilinear grid. The finite volume discretization for a component of the vector momenta along a ϕ face of a control volume is shown below:

$$\frac{\partial(\bar{p}_z)_{i,j,k}}{\partial t} = -\frac{1}{\Delta V_{i,j,k}} \left((\mathcal{T}_{rz})_{i+\frac{1}{2},j,k} - (\mathcal{T}_{rz})_{i-\frac{1}{2},j,k} + (\mathcal{T}_{\theta z})_{i,j+\frac{1}{2},k} - (\mathcal{T}_{\theta z})_{i,j-\frac{1}{2},k} \right. \\ \left. + (\mathcal{T}_{\phi z})_{i,j,k+\frac{1}{2}} - (\mathcal{T}_{\phi z})_{i,j,k-\frac{1}{2}} \right)$$

The rank-2 “numerical tensor functions” in this expression are given by

$$(\mathcal{T}_{rz})_{i-\frac{1}{2},j,k} = \left(\frac{1}{a_{i-\frac{1}{2},j,k}^+ - a_{i-\frac{1}{2},j,k}^-} \right) \int_{\theta_{j-1/2}}^{\theta_{j+1/2}} \int_{\phi_{k-1/2}}^{\phi_{k+1/2}} d\theta d\phi r_{i-\frac{1}{2}}^2 \sin \theta \left(-a_{i-\frac{1}{2},j,k}^- T_{rz}(u_{i,j,k}) \right. \\ \left. + a_{i-\frac{1}{2},j,k}^+ T_{rz}(u_{i-1,j,k}) - a_{i-\frac{1}{2},j,k}^- a_{i-\frac{1}{2},j,k}^+ (u_{i-1,j,k}^n - u_{i,j,k}^n) \right) |_{r_{i-\frac{1}{2}}}$$

$$(\mathcal{T}_{\theta z})_{i,j-\frac{1}{2},k} = \left(\frac{1}{b_{i,j-\frac{1}{2},k}^+ - b_{i,j-\frac{1}{2},k}^-} \right) \int_{r_{i-1/2}}^{r_{i+1/2}} \int_{\phi_{k-1/2}}^{\phi_{k+1/2}} dr d\phi r \sin \theta_{j-\frac{1}{2}} \left(-b_{i,j-\frac{1}{2},k}^- T_{\theta z}(u_{i,j,k}) \right. \\ \left. + b_{i,j-\frac{1}{2},k}^+ T_{\theta z}(u_{i,j-1,k}) - b_{i,j-\frac{1}{2},k}^- b_{i,j-\frac{1}{2},k}^+ (u_{i,j-1,k}^n - u_{i,j,k}^n) \right) |_{\theta_{j-\frac{1}{2}}}$$

$$(\mathcal{T}_{\phi z})_{i,j,k-\frac{1}{2}} = \left(\frac{1}{c_{i,j,k-\frac{1}{2}}^+ - c_{i,j,k-\frac{1}{2}}^-} \right) \int_{r_{i-1/2}}^{r_{i+1/2}} \int_{\theta_{j-1/2}}^{\theta_{j+1/2}} d\theta dr \left(-c_{i,j,k-\frac{1}{2}}^- T_{\phi z}(u_{i,j,k}) \right. \\ \left. + c_{i,j,k-\frac{1}{2}}^+ T_{\phi z}(u_{i,j,k-1}) - c_{i,j,k-\frac{1}{2}}^- c_{i,j,k-\frac{1}{2}}^+ (u_{i,j,k-1}^n - u_{i,j,k}^n) \right) |_{\phi_{k-\frac{1}{2}}}$$

Discretization and the 3D Semi-Discrete formalism

The numerical tensors are expressed in terms of the physical momentum fluxes normal to surfaces of the curvilinear mesh element. For our particular example they take the form:

$$T_{rz}(u_{i,j,k}) = \cos \theta_j T_{rr}(u_{i,j,k}) - \sin \theta_j T_{r\theta}(u_{i,j,k})$$

$$T_{\phi z}(u_{i,j,k}) = \cos \theta_j T_{\phi r}(u_{i,j,k}) - \sin \theta_j T_{\phi\theta}(u_{i,j,k})$$

$$T_{\theta z}(u_{i,j,k}) = \cos \theta_j T_{\theta r}(u_{i,j,k}) - \sin \theta_j T_{\theta\theta}(u_{i,j,k})$$

Finally, the explicit update is performed, and the state vector is updated:

$$(\overline{p_r})_{i,j,k} = \sin \theta_j \cos \phi_k (\overline{p_x})_{i,j,k} + \sin \theta_j \sin \phi_k (\overline{p_y})_{i,j,k} + \cos \theta_j (\overline{p_z})_{i,j,k}$$

$$(\overline{p_\theta})_{i,j,k} = \cos \theta_j \cos \phi_k (\overline{p_x})_{i,j,k} + \cos \theta_j \sin \phi_k (\overline{p_y})_{i,j,k} - \sin \theta_j (\overline{p_z})_{i,j,k}$$

$$(\overline{p_\phi})_{i,j,k} = -\sin \phi_k (\overline{p_x})_{i,j,k} + \cos \phi_k (\overline{p_y})_{i,j,k}$$

The integrals are calculated using a simple, high-order Gaussian interpolation, and point values of the physical momentum fluxes at cell faces are calculated from cell centers using piecewise-continuous, non-directionally split interpolation polynomials $\mathbf{T}(u_{i,j,k})$. Before discussing interpolations central to the method, we turn to the other vector equation of the MHD system: Faraday's Law.

Faraday's law, Constrained transport, and the solenoidal constraint:

$$\frac{1}{\Delta A} \int_A \frac{\partial \mathbf{B}}{\partial t} dA = \frac{1}{\Delta A} \int_A c (\nabla \times \mathbf{E}) dA = \frac{1}{\Delta A} \oint_C c \mathbf{E} \cdot d\mathbf{l}$$

The basic essence of any CT scheme is to simply define magnetic fields at cell faces, and update the components of the magnetic field in a quasi-2D fashion by taking the curl of the electric field along edges of a control volume. In principle, this ensures the divergence-free nature of the magnetic field accurate to numerical round-off error

However, ***the presence of discontinuities in the transverse components of the field at control volume surfaces presents a challenge in the context of a finite volume formalism over a generalized curvilinear mesh.*** There are three staggered regions where discontinuities may occur:

- *Corner regions can have discontinuities in two coordinate directions and involve four control volume cells;*
- *Edge regions can have discontinuities in one coordinate direction and involve two control volume cells;*
- *Central regions cannot have discontinuities and involve a single control volume.*

We extend the method of Kissmann and Pomoell (2012), and in Abbett & Bercik (2014) derive a ***semi-discrete, finite volume method of Constrained Transport (CT) on a fully-3D curvilinear grid.*** What follows is the the final form of the 3D discretization of Faraday's law above:

Faraday's law, Constrained transport, and the solenoidal constraint:

$$\frac{d\bar{B}_{r;i-\frac{1}{2},j,k}}{dt} = -\frac{1}{\Delta A_{i-\frac{1}{2},j,k}} \left(\int_{\phi_{k-\frac{1}{2}}}^{\phi_{k+\frac{1}{2}}} \mathbb{E}_{\phi;i-\frac{1}{2},j-\frac{1}{2},k} r_{i-\frac{1}{2}} \sin \theta_{j-\frac{1}{2}} d\phi + \int_{\phi_{k-\frac{1}{2}}}^{\phi_{k+\frac{1}{2}}} \mathbb{E}_{\phi;i-\frac{1}{2},j+\frac{1}{2},k} r_{i-\frac{1}{2}} \sin \theta_{j+\frac{1}{2}} d\phi \right. \\ \left. + \int_{\theta_{j-\frac{1}{2}}}^{\theta_{j+\frac{1}{2}}} \mathbb{E}_{\theta;i-\frac{1}{2},j,k-\frac{1}{2}} r_{i-\frac{1}{2}} d\theta + \int_{\theta_{j-\frac{1}{2}}}^{\theta_{j+\frac{1}{2}}} \mathbb{E}_{\theta;i-\frac{1}{2},j,k+\frac{1}{2}} r_{i-\frac{1}{2}} d\theta \right)$$

$$\frac{d\bar{B}_{\theta;i,j-\frac{1}{2},k}}{dt} = -\frac{1}{\Delta A_{i,j-\frac{1}{2},k}} \left(\int_{\phi_{k-\frac{1}{2}}}^{\phi_{k+\frac{1}{2}}} \mathbb{E}_{\phi;i-\frac{1}{2},j-\frac{1}{2},k} r_{i-\frac{1}{2}} \sin \theta_{j-\frac{1}{2}} d\phi + \int_{\phi_{k-\frac{1}{2}}}^{\phi_{k+\frac{1}{2}}} \mathbb{E}_{\phi;i+\frac{1}{2},j-\frac{1}{2},k} r_{i+\frac{1}{2}} \sin \theta_{j-\frac{1}{2}} d\phi \right. \\ \left. + \int_{r_{i-\frac{1}{2}}}^{r_{i+\frac{1}{2}}} \mathbb{E}_{r;i,j-\frac{1}{2},k-\frac{1}{2}} dr + \int_{r_{i-\frac{1}{2}}}^{r_{i+\frac{1}{2}}} \mathbb{E}_{r;i,j-\frac{1}{2},k+\frac{1}{2}} dr \right)$$

$$\frac{d\bar{B}_{\phi;i,j,k-\frac{1}{2}}}{dt} = -\frac{1}{\Delta A_{i,j,k-\frac{1}{2}}} \left(\int_{\theta_{j-\frac{1}{2}}}^{\theta_{j+\frac{1}{2}}} \mathbb{E}_{\theta;i-\frac{1}{2},j,k-\frac{1}{2}} r_{i-\frac{1}{2}} d\theta + \int_{\theta_{j-\frac{1}{2}}}^{\theta_{j+\frac{1}{2}}} \mathbb{E}_{\theta;i+\frac{1}{2},j,k-\frac{1}{2}} r_{i+\frac{1}{2}} d\theta \right. \\ \left. + \int_{r_{i-\frac{1}{2}}}^{r_{i+\frac{1}{2}}} \mathbb{E}_{r;i,j-\frac{1}{2},k-\frac{1}{2}} dr + \int_{r_{i-\frac{1}{2}}}^{r_{i+\frac{1}{2}}} \mathbb{E}_{r;i,j+\frac{1}{2},k-\frac{1}{2}} dr \right)$$

Integrals are calculated numerically using Gaussian integration along the edges of the control volume, and the electric fields here are numerical constructions that propagate transverse discontinuities.

Faraday's law, Constrained transport, and the solenoidal constraint:

Where the numerical representation of electric fields along cell edges take into account discontinuities in each transverse direction. For example, the ϕ component takes the form:

$$\mathbb{E}_{\phi; i-\frac{1}{2}, j-\frac{1}{2}, k} = \left(\frac{1}{a_{i-\frac{1}{2}, j-\frac{1}{2}, k}^+ - a_{i-\frac{1}{2}, j-\frac{1}{2}, k}^-} \right) \left(\frac{1}{b_{i-\frac{1}{2}, j-\frac{1}{2}, k}^+ - b_{i-\frac{1}{2}, j-\frac{1}{2}, k}^-} \right)$$

$$\left(a_{i-\frac{1}{2}, j-\frac{1}{2}, k}^- b_{i-\frac{1}{2}, j-\frac{1}{2}, k}^- E_{\phi; i-\frac{1}{2}, j-\frac{1}{2}, k}(u_{i, j, k}) - a_{i-\frac{1}{2}, j-\frac{1}{2}, k}^- b_{i-\frac{1}{2}, j-\frac{1}{2}, k}^+ E_{\phi; i-\frac{1}{2}, j-\frac{1}{2}, k}(u_{i, j-1, k}) - \right.$$

$$\left. a_{i-\frac{1}{2}, j-\frac{1}{2}, k}^+ b_{i-\frac{1}{2}, j-\frac{1}{2}, k}^- E_{\phi; i-\frac{1}{2}, j-\frac{1}{2}, k}(u_{i-1, j, k}) + a_{i-\frac{1}{2}, j-\frac{1}{2}, k}^+ b_{i-\frac{1}{2}, j-\frac{1}{2}, k}^+ E_{\phi; i-\frac{1}{2}, j-\frac{1}{2}, k}(u_{i-1, j-1, k}) \right) -$$

$$\left(\frac{a_{i-\frac{1}{2}, j-\frac{1}{2}, k}^- a_{i-\frac{1}{2}, j-\frac{1}{2}, k}^+}{a_{i-\frac{1}{2}, j-\frac{1}{2}, k}^+ - a_{i-\frac{1}{2}, j-\frac{1}{2}, k}^-} \right) \left(B_{\theta; i, j-\frac{1}{2}, k}^n - B_{\theta; i-1, j-\frac{1}{2}, k}^n \right) + \left(\frac{b_{i-\frac{1}{2}, j-\frac{1}{2}, k}^+ b_{i-\frac{1}{2}, j-\frac{1}{2}, k}^-}{b_{i-\frac{1}{2}, j-\frac{1}{2}, k}^+ - b_{i-\frac{1}{2}, j-\frac{1}{2}, k}^-} \right) \left(B_{r; i-\frac{1}{2}, j, k}^n - B_{r; i-\frac{1}{2}, j-1, k}^n \right)$$

We now require volume-averaged values at cell centers in order to properly evaluate point values of (1) Maxwell stresses and Lorentz forces; and (2) point values of magnetoacoustic wave speeds along faces of the control volume (used in the integral update of the vector momentum conservation equation).

Faraday's law, Constrained transport, and the solenoidal constraint:

One cannot interpolate face-averaged components of the magnetic field to obtain their volume averaged cell-centered counterparts in a way that is mathematically consistent with our formalism. *We must therefore evolve volume-centered averages using CT electric fields:*

$$\frac{1}{\Delta V} \int_V \frac{\partial \mathbf{B}}{\partial t} dV = -\frac{1}{\Delta V} \int_V c(\nabla \times \mathbf{E}) dV = -\frac{1}{\Delta V} \oint_A c(\hat{\mathbf{n}} \times \mathbf{E}) dA$$

The above governing equation is used to discretize the vector induction equation, and numerical integrations use the same CT electric fields along cell averages that are used to update the face-centered components of the magnetic field. Thus, **volume centered quantities are fully consistent with the CT scheme**, and the solenoidal constraint is maintained to numerical roundoff. Solutions take the form:

$$\begin{aligned} \frac{\partial}{\partial t} \overline{B_x}(r, \theta, \phi) &= \frac{1}{\Delta V} \int_{A_r^L} [-\cos(\theta) \cos(\phi) c E_\phi(r, \theta, \phi) - \sin(\phi) c E_\theta(r, \theta, \phi)] dA_r - \\ &\frac{1}{\Delta V} \int_{A_r^U} [-\cos(\theta) \cos(\phi) c E_\phi(r, \theta, \phi) - \sin(\phi) c E_\theta(r, \theta, \phi)] dA_r + \\ &\frac{1}{\Delta V} \int_{A_\theta^L} [\sin(\theta) \cos(\phi) c E_\phi(r, \theta, \phi) + \sin(\phi) c E_r(r, \theta, \phi)] dA_\theta - \\ &\frac{1}{\Delta V} \int_{A_\theta^U} [\sin(\theta) \cos(\phi) c E_\phi(r, \theta, \phi) + \sin(\phi) c E_r(r, \theta, \phi)] dA_\theta + \\ &\frac{1}{\Delta V} \int_{A_\phi^L} [-\sin(\theta) \cos(\phi) c E_\theta(r, \theta, \phi) + \cos(\theta) \cos(\phi) c E_r(r, \theta, \phi)] dA_\phi - \\ &\frac{1}{\Delta V} \int_{A_\phi^U} [-\sin(\theta) \cos(\phi) c E_\theta(r, \theta, \phi) + \cos(\theta) \cos(\phi) c E_r(r, \theta, \phi)] dA_\phi \end{aligned}$$

Faraday's law, Constrained transport, and the solenoidal constraint:

And the other components take the form:

$$\begin{aligned}
 \frac{\partial}{\partial t} \overline{B}_y(r, \theta, \phi) = & \frac{1}{\Delta V} \int_{A_r^L} [-\cos(\theta) \sin(\phi) c E_\phi(r, \theta, \phi) + \cos(\phi) c E_\theta(r, \theta, \phi)] dA_r - \\
 & \frac{1}{\Delta V} \int_{A_r^U} [-\cos(\theta) \sin(\phi) c E_\phi(r, \theta, \phi) + \cos(\phi) c E_\theta(r, \theta, \phi)] dA_r + \\
 & \frac{1}{\Delta V} \int_{A_\theta^L} [\sin(\theta) \sin(\phi) c E_\phi(r, \theta, \phi) - \cos(\phi) c E_r(r, \theta, \phi)] dA_\theta - \\
 & \frac{1}{\Delta V} \int_{A_\theta^U} [\sin(\theta) \sin(\phi) c E_\phi(r, \theta, \phi) - \cos(\phi) c E_r(r, \theta, \phi)] dA_\theta + \\
 & \frac{1}{\Delta V} \int_{A_\phi^L} [-\sin(\theta) \sin(\phi) c E_\theta(r, \theta, \phi) + \cos(\theta) \sin(\phi) c E_r(r, \theta, \phi)] dA_\phi - \\
 & \frac{1}{\Delta V} \int_{A_\phi^U} [-\sin(\theta) \sin(\phi) c E_\theta(r, \theta, \phi) + \cos(\theta) \sin(\phi) c E_r(r, \theta, \phi)] dA_\phi
 \end{aligned}$$

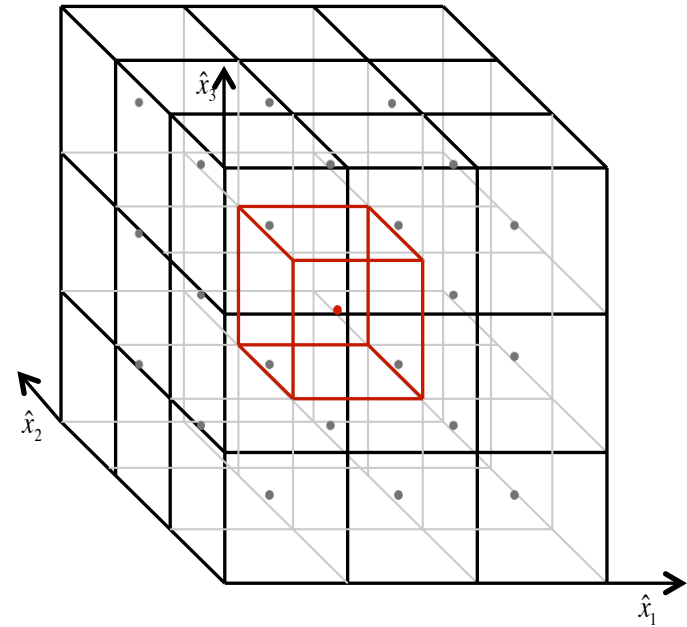
$$\begin{aligned}
 \frac{\partial}{\partial t} \overline{B}_z(r, \theta, \phi) = & \frac{1}{\Delta V} \int_{A_r^L} [\sin(\theta) c E_\phi(r, \theta, \phi)] dA_r - \frac{1}{\Delta V} \int_{A_r^U} [\sin(\theta) c E_\phi(r, \theta, \phi)] dA_r + \\
 & \frac{1}{\Delta V} \int_{A_\theta^L} [\cos(\theta) c E_\phi(r, \theta, \phi)] dA_\theta - \frac{1}{\Delta V} \int_{A_\theta^U} [\cos(\theta) c E_\phi(r, \theta, \phi)] dA_\theta + \\
 & \frac{1}{\Delta V} \int_{A_\phi^L} [-\cos(\theta) c E_\theta(r, \theta, \phi) - \sin(\theta) c E_r(r, \theta, \phi)] dA_\phi - \frac{1}{\Delta V} \int_{A_\phi^U} [-\cos(\theta) c E_\theta(r, \theta, \phi) - \sin(\theta) c E_r(r, \theta, \phi)] dA_\phi
 \end{aligned}$$

Once integrated and updated, the field is projected to the base coordinate system.

Piecewise continuous high-order fully-3D polynomial interpolation:

To evaluate the previous integrals, and calculate high-order fluxes and electric fields along faces and edges of a curvilinear control volume, we utilize a *non-directionally split 27-point 3D stencil* of cell-centered quantities determined from the following interpolating polynomial (based on a 3D Taylor expansion).

$$\begin{aligned}
 q_{i,j,k}(r,\theta,\phi) = & a_1 + a_2(r-r_i) + a_3r_i(\theta-\theta_j) + a_4r_i\sin\theta_j(\phi-\phi_k) + a_5(r-r_i)^2 \\
 & + a_6r_i^2(\theta-\theta_j)^2 + a_7r_i^2\sin^2\theta_j(\phi-\phi_k)^2 + a_8(r-r_i)r_i(\theta-\theta_j) \\
 & + a_9(r-r_i)r_i\sin\theta_j(\phi-\phi_k) + a_{10}r_i(\theta-\theta_j)r_i\sin\theta_j(\phi-\phi_k) \\
 & + a_{11}(r-r_i)^2r_i(\theta-\theta_j) + a_{12}(r-r_i)^2r_i\sin\theta_j(\phi-\phi_k) \\
 & + a_{13}(r-r_i)r_i^2(\theta-\theta_j)^2 + a_{14}r_i^2(\theta-\theta_j)^2r_i\sin\theta_j(\phi-\phi_k) \\
 & + a_{15}(r-r_i)r_i^2\sin^2\theta_j(\phi-\phi_k)^2 + a_{16}r_i(\theta-\theta_j)r_i^2\sin^2\theta_j(\phi-\phi_k)^2 \\
 & + a_{17}(r-r_i)r_i(\theta-\theta_j)r_i\sin\theta_j(\phi-\phi_k) + a_{18}(r-r_i)^2r_i^2(\theta-\theta_j)^2 \\
 & + a_{19}(r-r_i)^2r_i^2\sin^2\theta_j(\phi-\phi_k)^2 + a_{20}r_i^2(\theta-\theta_j)^2r_i^2\sin^2\theta_j(\phi-\phi_k)^2 \\
 & + a_{21}(r-r_i)^2r_i(\theta-\theta_j)r_i\sin\theta_j(\phi-\phi_k) + a_{22}(r-r_i)r_i^2(\theta-\theta_j)^2r_i\sin\theta_j(\phi-\phi_k) \\
 & + a_{23}(r-r_i)r_i(\theta-\theta_j)r_i^2\sin^2\theta_j(\phi-\phi_k)^2 + a_{24}(r-r_i)^2r_i^2(\theta-\theta_j)^2r_i\sin\theta_j(\phi-\phi_k) \\
 & + a_{25}(r-r_i)^2r_i(\theta-\theta_j)r_i^2\sin^2\theta_j(\phi-\phi_k)^2 + a_{26}(r-r_i)r_i^2(\theta-\theta_j)^2r_i^2\sin^2\theta_j(\phi-\phi_k)^2 \\
 & + a_{27}(r-r_i)^2r_i^2(\theta-\theta_j)^2r_i^2\sin^2\theta_j(\phi-\phi_k)^2
 \end{aligned}$$



The stencil is determined by enforcing the definition of cell-averages in either spherical or Cartesian geometries (for spherical geometries $x = r, y = \theta, z = \phi$) :

$$\bar{q}_{i+l,j+m,k+n} = \frac{1}{\Delta V} \int_{x_{i-1/2}+l\Delta x}^{x_{i+1/2}+l\Delta x} \int_{y_{j-1/2}+m\Delta y}^{y_{j+1/2}+m\Delta y} \int_{z_{k-1/2}-n\Delta z}^{z_{k+1/2}+n\Delta z} q_{i,j,k}(x,y,z) dV \quad l,m,n = -1,0,1$$

Substituting the previous Taylor polynomial into this expression, and evaluating it for all 27 surrounding points (shown in the figure) yields an invertable system of equations for the coefficients a_j in terms of known, cell-centered quantities. It is important to note that the integrations must be carried out in *physical space*, where

$$\Delta V(i,j,k;l,m,n) = \int_{x_{i-1/2}+l\Delta x}^{x_{i+1/2}+l\Delta x} \int_{y_{j-1/2}+m\Delta y}^{y_{j+1/2}+m\Delta y} \int_{z_{k-1/2}-n\Delta z}^{z_{k+1/2}+n\Delta z} dV \quad l,m,n = -1,0,1$$

$$dV = \begin{cases} dx dy dz & \text{Cartesian} \\ r^2 \sin \theta dr d\theta d\phi & \text{spherical} \end{cases}$$

Once the system is inverted and the stencil determined for each coefficient of the Taylor polynomial, we have the high-order interpolating polynomial necessary to specify the components of the MHD state vector at each face of any control volume in terms of known, discrete, centered, cell-averaged quantities.

Advantages of the fully 3D approach:

High accuracy --- important for large-scale calculations where high-resolution becomes computationally expensive

Prevent grid anisotropies --- important to not introduce off-axis, anisotropic grid diffusion, thus preventing non-physical reconnections and variations in resistive and viscous heating

Maintains symmetries independent of the choice of coordinate systems --- i.e., spherical waves are more accurately represented in Cartesian grids, and planar waves are more accurately represented in spherical grids

Eliminates unphysical alignments: Eliminates possibility of spurious alignments of features along coordinate axes

Inexpensive: Surprisingly, the approach is computationally efficient, and compares well with the directionally-split scheme.

Direct Stabilization:

All codes require some form of stabilization; for our high-order formalism, this need is most apparent near shock fronts. The key is to employ a stabilization scheme that is robust, yet preserves the high-order nature of the solution away from shock fronts. We developed the following method called *Direct Stabilization (DS)*, since it uses a direct measure of calculated discontinuities in components of the state vector at each integration point along control volume faces. The interpolating polynomial is cast in terms of both a high order polynomial, and a low-order stabilizing term:

$$q_{i,j,k}(r, \theta, \phi, t) = w^L q_{i,j,k}^L(r, \theta, \phi, t) + w^H q_{i,j,k}^H(r, \theta, \phi, t)$$

where

$$w^L = \frac{w_0}{w_1 + w_0}$$

$$w^H = \frac{w_1}{w_1 + w_0}$$

$$w_0 = \frac{1}{(\delta^L + \varepsilon_1 q_n^L + \varepsilon_2)^p}$$

$$w_1 = \frac{1}{(\delta^H + \varepsilon_1 q_n^H + \varepsilon_2)^p}$$

$$\delta^L = \left| q_{i,j,k}^L(r_{i-1/2}, \theta_j, \phi_k) - q_{i-1,j,k}^L(r_{i-1/2}, \theta_j, \phi_k) \right|$$

$$\delta^H = \left| q_{i,j,k}^H(r_{i-1/2}, \theta_j, \phi_k) - q_{i-1,j,k}^H(r_{i-1/2}, \theta_j, \phi_k) \right|$$

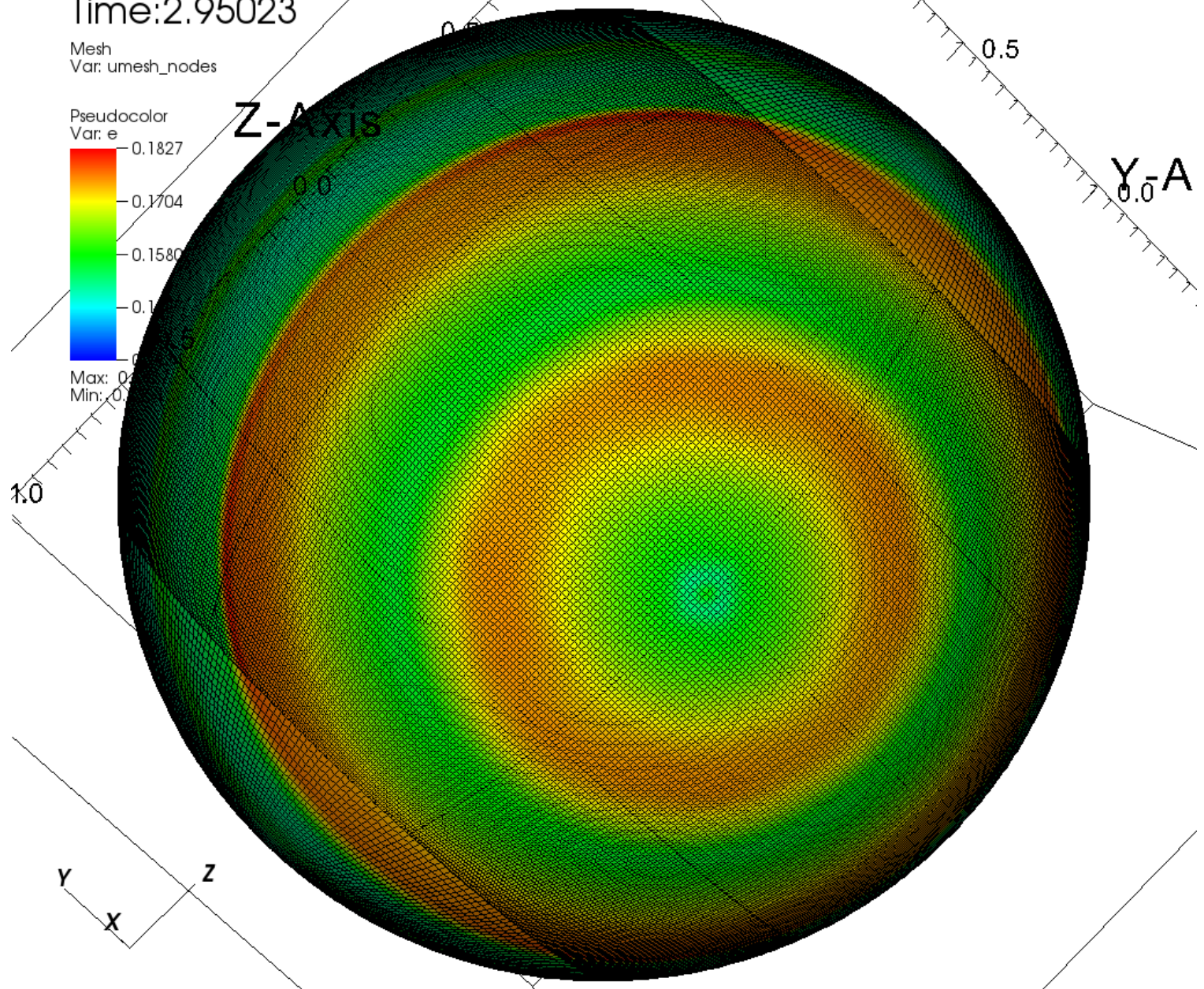
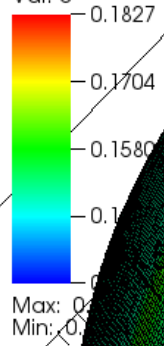
$$q_n^L = \sqrt{\left(q_{i,j,k}^L(r_{i-1/2}, \theta_j, \phi_k) \right)^2 + \left(q_{i-1,j,k}^L(r_{i-1/2}, \theta_j, \phi_k) \right)^2}$$

$$q_n^H = \sqrt{\left(q_{i,j,k}^H(r_{i-1/2}, \theta_j, \phi_k) \right)^2 + \left(q_{i-1,j,k}^H(r_{i-1/2}, \theta_j, \phi_k) \right)^2}$$

DB: spherical-blast-2level_visit_0150_reflvl_0.sdf
Time: 2.95023

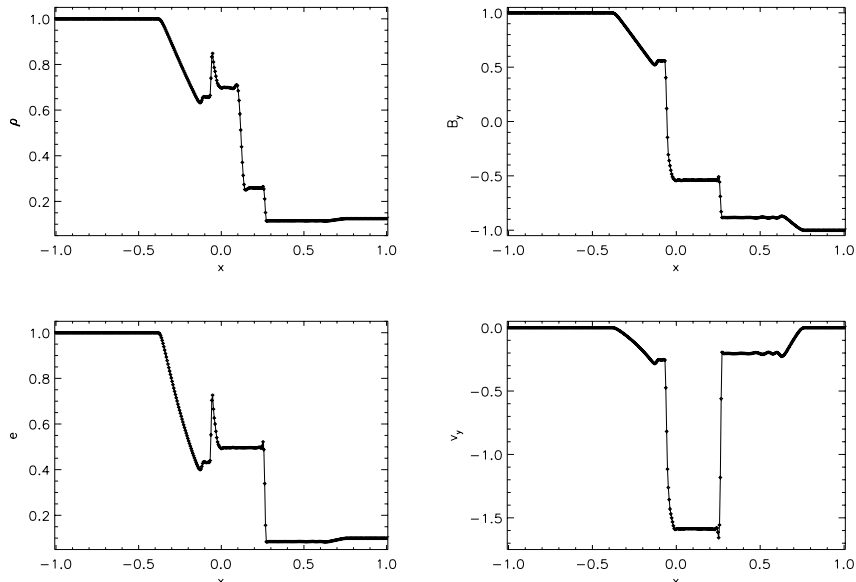
Mesh
Var: umesh_nodes

Pseudocolor
Var: e

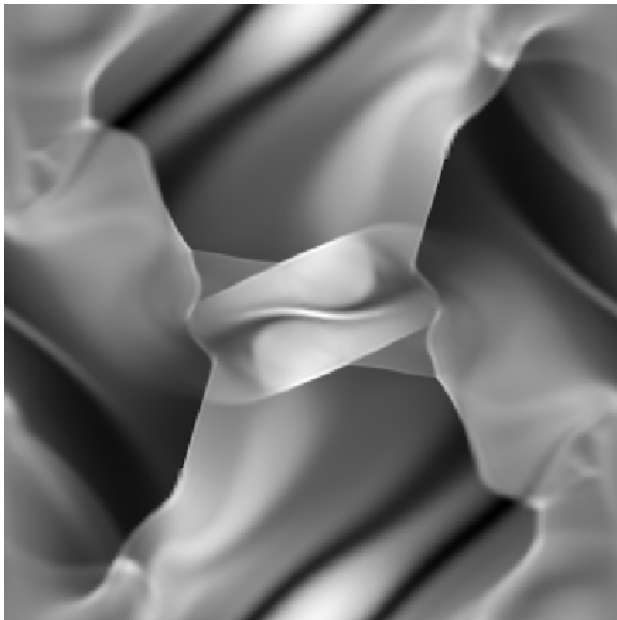


Addressing the challenge of robustness:

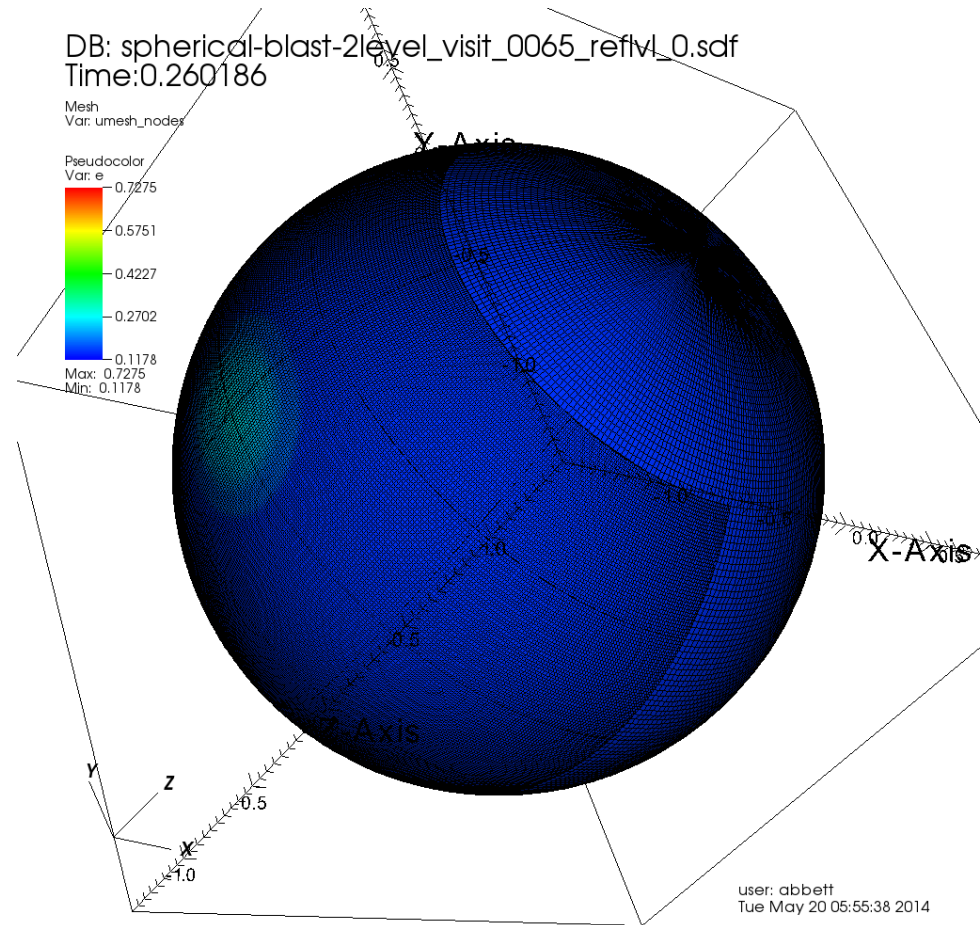
Test, test, and test some more....



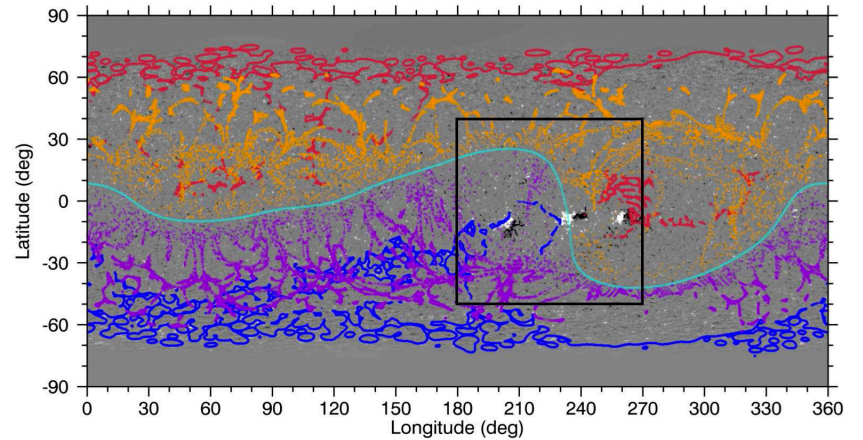
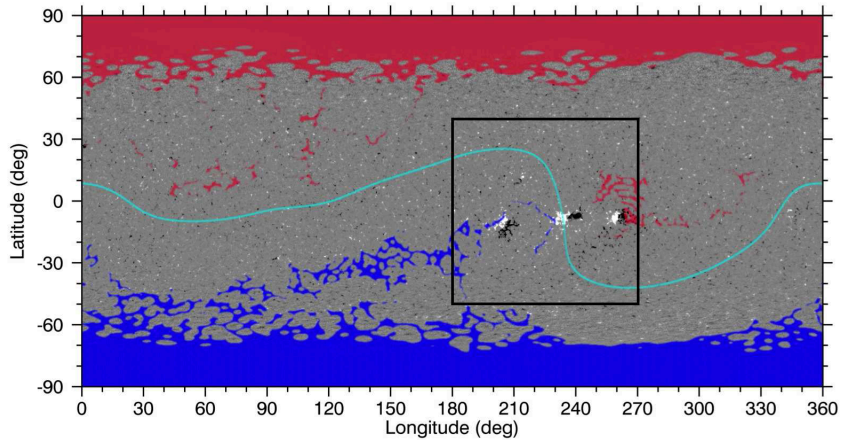
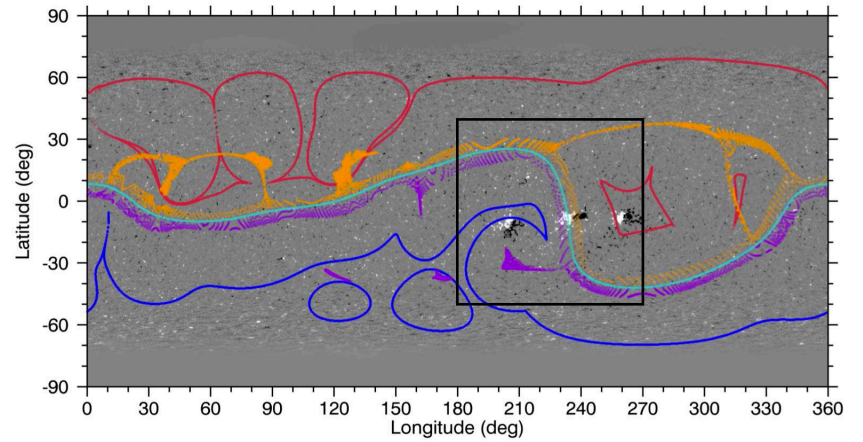
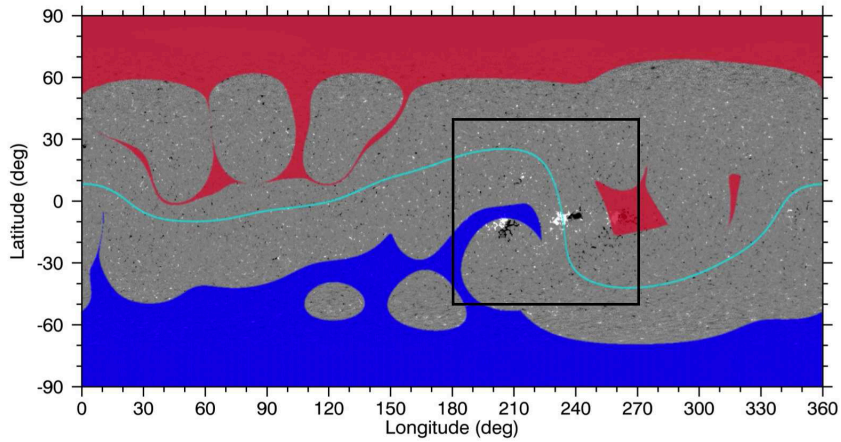
Off-axis 1D symmetric MHD shocks



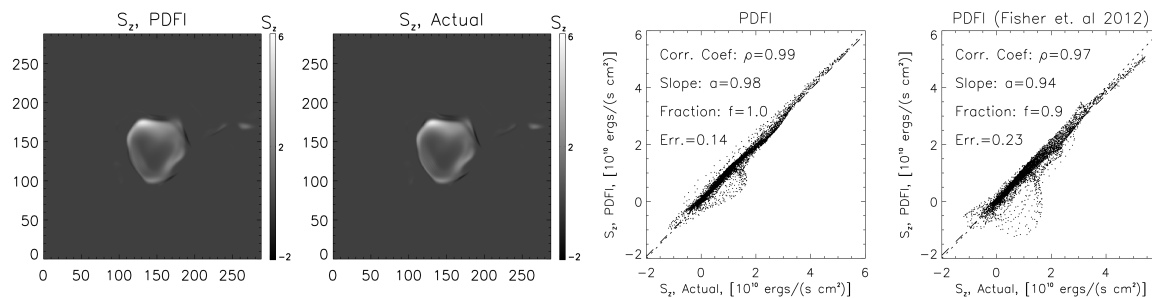
MHD turbulence at multiple refinement levels



High Mach number MHD shocks



Bercik et al., (2014)



Kazachenko et al., (2014)

Initial global configurations and the driving boundary: The challenge of “relaxation”

Conclusion:

We have successfully developed, and are currently testing the properties of a new version of the RADMHD software with the capability to perform global calculations at non-uniform resolution in spherical geometries. The numerical scheme has been updated to incorporate a high-order fully-3D non-directionally split stencil in the explicit sub-step to enhance accuracy in large-scale calculations where spatial resolution is at a premium.

While non-uniform gridding is an invaluable tool, and now commonplace in large-scale MHD codes (including this one), the challenging nature of evolving surface convection coupled with large-scale phenomena in the solar atmosphere (and the disparate temporal and spatial scales involved) compelled us to also revisit the base numerical schemes of our code.

We have now progressed to the point where global and active region-scale simulations in a high-resolution, dynamically evolving, global magnetic field can be initiated. We are currently relaxing a convective state and coupled atmosphere in a large-scale spherical wedge using the new formalism, and will report on the results in the near future.